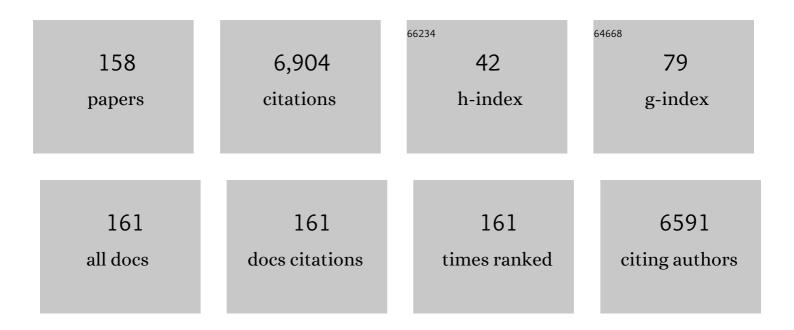
Jonathan D Poplawsky

List of Publications by Year in descending order

Source: https://exaly.com/author-pdf/4441437/publications.pdf Version: 2024-02-01



#	Article	IF	CITATIONS
1	Nano-scale insights regarding coke formation in zeolite SSZ-13 subject to the methanol-to-hydrocarbons reaction. Catalysis Science and Technology, 2022, 12, 1220-1228.	2.1	13
2	Measuring oxygen solubility in Ni grains and boundaries after oxidation using atom probe tomography. Scripta Materialia, 2022, 210, 114411.	2.6	6
3	Biocompatibility of NbTaTiVZr with Surface Modifications for Osteoblasts. ACS Applied Bio Materials, 2022, 5, 642-649.	2.3	1
4	A creep-resistant additively manufactured Al-Ce-Ni-Mn alloy. Acta Materialia, 2022, 227, 117699.	3.8	51
5	Microstructural evolution and strengthening mechanisms in a heat-treated additively manufactured Al–Cu–Mn–Zr alloy. Materials Science & Engineering A: Structural Materials: Properties, Microstructure and Processing, 2022, 840, 142928.	2.6	15
6	Effect of heavy ion irradiation dose rate and temperature on α′ precipitation in high purity Fe-18%Cr alloy. Acta Materialia, 2022, 231, 117888. Medeling of the Thermodiffusion Induced Filement Formation in complimath	3.8	9
7	xmlns:mml="http://www.w3.org/1998/Math/MathML" display="inline" overflow="scroll"> <mml:mrow><mml:mi>Ti</mml:mi><mml:mi mathvariant="normal">N</mml:mi </mml:mrow> <mml:mo>/</mml:mo> <mml:msub><mml:mi>Ta</mml:mi><m mathvariant="normal">O<mml:mrow><mml:mrow><mml:mrow></mml:mrow></mml:mrow></mml:mrow><td>ml<mark>1.5</mark>i>xâ^'<td>ກສໍl:mi><!--ຫ<br-->າວ><mml:mi< td=""></mml:mi<></td></td></m </mml:msub>	ml <mark>1.5</mark> i>xâ^' <td>ກສໍl:mi><!--ຫ<br-->າວ><mml:mi< td=""></mml:mi<></td>	ກສໍl:mi> ຫ<br າວ> <mml:mi< td=""></mml:mi<>
8	Understanding effects of chemical complexity on helium bubble formation in Ni-based concentrated solid solution alloys based on elemental segregation measurements. Journal of Nuclear Materials, 2022, 569, 153902.	1.3	4
9	Aging behavior and strengthening mechanisms of coarsening resistant metastable Î,' precipitates in an Al–Cu alloy. Materials and Design, 2021, 198, 109378.	3.3	62
10	Effects of niobium and tantalum on the microstructure and strength of ferritic-martensitic steels. Materials Science & Engineering A: Structural Materials: Properties, Microstructure and Processing, 2021, 807, 140900.	2.6	9
11	Examining the creep strengthening nanoprecipitation in novel highly reinforced heat resistant steels. Materials Characterization, 2021, 174, 110982.	1.9	4
12	The subsurface structure of abraded Al–Zn–Mg–Cu alloy. Materialia, 2021, 16, 101065.	1.3	1
13	The role of Si in determining the stability of the Î,′ precipitate in Al-Cu-Mn-Zr alloys. Journal of Alloys and Compounds, 2021, 862, 158152.	2.8	22
14	Correlating advanced microscopies reveals atomic-scale mechanisms limiting lithium-ion battery lifetime. Nature Communications, 2021, 12, 3740.	5.8	6
15	Atomic structures of interfacial solute gateways to Î,′ precipitates in Al-Cu alloys. Acta Materialia, 2021, 212, 116891.	3.8	18
16	Bifunctional nanoprecipitates strengthen and ductilize a medium-entropy alloy. Nature, 2021, 595, 245-249.	13.7	141
17	Understanding the influence of grain size on α' Cr precipitation in Fe-21Cr-5Al alloy during thermal aging using atom probe tomography. Microscopy and Microanalysis, 2021, 27, 3380-3382.	0.2	1
18	High-throughput design of high-performance lightweight high-entropy alloys. Nature Communications, 2021, 12, 4329.	5.8	112

#	Article	IF	CITATIONS
19	Nanoscale Chemical Imaging in Zeolite Catalysts by Atom Probe Tomography. Microscopy and Microanalysis, 2021, 27, 984-985.	0.2	0
20	Nanoscale Analysis of LSM/YSZ Interfaces within Composite Cathodes for Commercial Solid Oxide Fuel Cells. ECS Transactions, 2021, 103, 1351-1362.	0.3	1
21	The detrimental effect of elemental contaminants when using B additions to improve the creep properties of a Ni-based superalloy. Scripta Materialia, 2021, 201, 113971.	2.6	7
22	Strength can be controlled by edge dislocations in refractory high-entropy alloys. Nature Communications, 2021, 12, 5474.	5.8	64
23	High radiation tolerance of an ultrastrong nanostructured NiCoCr alloy with stable dispersed nanooxides and fine grain structure. Journal of Nuclear Materials, 2021, 557, 153316.	1.3	11
24	Gradient cell–structured high-entropy alloy with exceptional strength and ductility. Science, 2021, 374, 984-989.	6.0	316
25	Influence of artificial aging on corrosion of abraded Al-Zn-Mg-Cu alloys. Corrosion Science, 2021, 191, 109745.	3.0	4
26	Elevated temperature ductility dip in an additively manufactured Al-Cu-Ce alloy. Acta Materialia, 2021, 220, 117285.	3.8	38
27	Understanding the microstructural stability in a γ′-strengthened Ni-Fe-Cr-Al-Ti alloy. Journal of Alloys and Compounds, 2021, 886, 161207.	2.8	1
28	Superior Highâ€Temperature Strength in a Supersaturated Refractory Highâ€Entropy Alloy. Advanced Materials, 2021, 33, e2102401.	11.1	89
29	Examining the multi-scale complexity and the crystallographic hierarchy of isothermally treated bainitic and martensitic structures. Materials Characterization, 2020, 160, 110127.	1.9	8
30	Radiation response of a Fe–20Cr–25Ni austenitic stainless steel under Fe2+ irradiation at 500°C. Materialia, 2020, 9, 100542.	1.3	8
31	Fabrication and Characterization of Composite Membranes for the Concentration of Lithium Containing Solutions Using Forward Osmosis. Advanced Sustainable Systems, 2020, 4, 2000165.	2.7	5
32	Irradiation-induced segregation at dislocation loops in CoCrFeMnNi high entropy alloy. Materialia, 2020, 14, 100951.	1.3	18
33	Partitioning of tramp elements Cu and Si in a Ni-based superalloy and their effect on creep properties. Materialia, 2020, 13, 100843.	1.3	7
34	Latticeâ€Distortionâ€Enhanced Yield Strength in a Refractory Highâ€Entropy Alloy. Advanced Materials, 2020, 32, e2004029.	11.1	121
35	Perspectives on Quenching and Tempering 4340 Steel. Metallurgical and Materials Transactions A: Physical Metallurgy and Materials Science, 2020, 51, 4984-5005.	1.1	34
36	Localized corrosion at nm-scale hardening precipitates in Al-Cu-Li alloys. Acta Materialia, 2020, 189, 204-213.	3.8	43

#	Article	IF	CITATIONS
37	Colossal oxygen vacancy formation at a fluorite-bixbyite interface. Nature Communications, 2020, 11, 1371.	5.8	39
38	Structural damage and phase stability of Al0.3CoCrFeNi high entropy alloy under high temperature ion irradiation. Acta Materialia, 2020, 188, 1-15.	3.8	83
39	Coupling computational thermodynamics with density-function-theory based calculations to design L12 precipitates in Fe Ni based alloys. Materials and Design, 2020, 191, 108592.	3.3	5
40	Probing Heterogeneity in Bovine Enamel Composition through Nanoscale Chemical Imaging using Atom Probe Tomography. Archives of Oral Biology, 2020, 112, 104682.	0.8	4
41	Interpreting nanovoids in atom probe tomography data for accurate local compositional measurements. Nature Communications, 2020, 11, 1022.	5.8	23
42	Directly Linking Low-Angle Grain Boundary Misorientation to Device Functionality for GaAs Grown on Flexible Metal Substrates. ACS Applied Materials & Interfaces, 2020, 12, 10664-10672.	4.0	4
43	The synergistic role of Mn and Zr/Ti in producing Î,′/L12 co-precipitates in Al-Cu alloys. Acta Materialia, 2020, 194, 577-586.	3.8	71
44	The origin of passivity in aluminum-manganese solid solutions. Corrosion Science, 2020, 173, 108749.	3.0	22
45	Strong crystal field splitting and polarization dependence observed in the emission from Eu3+ ions doped into GaN. , 2020, , .		3
46	Interpreting Voids in Atom Probe Tomography Data via Experiment and Theory. Microscopy and Microanalysis, 2019, 25, 290-291.	0.2	0
47	In-situ TEM analysis of the phase transformation mechanism of a Cu–Al–Ni shape memory alloy. Journal of Alloys and Compounds, 2019, 808, 151743.	2.8	9
48	Elevated temperature microstructural stability in cast AlCuMnZr alloys through solute segregation. Materials Science & Engineering A: Structural Materials: Properties, Microstructure and Processing, 2019, 765, 138279.	2.6	89
49	Investigating Effects of Alloy Chemical Complexity on Helium Bubble Formation by Accurate Segregation Measurements Using Atom Probe Tomography. Microscopy and Microanalysis, 2019, 25, 1558-1559.	0.2	6
50	The Utility of Xe-Plasma FIB for Preparing Aluminum Alloy Specimens for MEMS-based In Situ Double-Tilt Heating Experiments. Microscopy and Microanalysis, 2019, 25, 1442-1443.	0.2	0
51	Validation of an alloy design strategy for stable Fe–Cr–Al–Nb-X ferritic alloys using electron microscopy and atom probe tomography. Materials Characterization, 2019, 158, 109987.	1.9	12
52	Structural, band and electrical characterization of β-(Al0.19Ga0.81)2O3 films grown by molecular beam epitaxy on Sn doped β-Ga2O3 substrate. Journal of Applied Physics, 2019, 126, .	1.1	26
53	Multi-modal characterization approach to understand proton transport mechanisms in solid oxide fuel cells. Microscopy and Microanalysis, 2019, 25, 2048-2049.	0.2	0
54	Peierls barrier characteristic and anomalous strain hardening provoked by dynamic-strain-aging strengthening in a body-centered-cubic high-entropy alloy. Materials Research Letters, 2019, 7, 475-481.	4.1	29

#	Article	IF	CITATIONS
55	Direct observation of creep strengthening nanoprecipitate formation in ausformed ferritic/martensitic steels. Scripta Materialia, 2019, 164, 76-81.	2.6	10
56	Understanding Mechanical Properties of Nano-Grained Bainitic Steels from Multiscale Structural Analysis. Metals, 2019, 9, 426.	1.0	8
57	Stable Metallic Enrichment in Conductive Filaments in TaO <i>_x</i> â€Based Resistive Switches Arising from Competing Diffusive Fluxes. Advanced Electronic Materials, 2019, 5, 1800954.	2.6	28
58	Mechanisms for stabilizing Î,′(Al2Cu) precipitates at elevated temperatures investigated with phase field modeling. Materialia, 2019, 6, 100335.	1.3	31
59	Cascading microstructures in aluminum-steel interfaces created by impact welding. Materials Characterization, 2019, 151, 119-128.	1.9	17
60	Shape-preserving machining produces gradient nanolaminate medium entropy alloys with high strain hardening capability. Acta Materialia, 2019, 170, 176-186.	3.8	41
61	Cascading phase transformations in high carbon steel resulting in the formation of inverse bainite: An atomic scale investigation. Scientific Reports, 2019, 9, 5597.	1.6	2
62	Phase transformations of HfNbTaTiZr high-entropy alloy at intermediate temperatures. Scripta Materialia, 2019, 158, 50-56.	2.6	139
63	Probing the Location and Speciation of Elements in Zeolites with Correlated Atom Probe Tomography and Scanning Transmission Xâ€Ray Microscopy. ChemCatChem, 2019, 11, 488-494.	1.8	19
64	Novel NiAl-strengthened high entropy alloys with balanced tensile strength and ductility. Materials Science & Engineering A: Structural Materials: Properties, Microstructure and Processing, 2019, 742, 636-647.	2.6	44
65	Influence of Alloying on α-αʹ Phase Separation in Duplex Stainless Steels. Minerals, Metals and Materials Series, 2019, , 2399-2408.	0.3	1
66	Extremely hard amorphous-crystalline hybrid steel surface produced by deformation induced cementite amorphization. Acta Materialia, 2018, 152, 107-118.	3.8	13
67	Investigation of pre-existing particles in Al 5083 alloys. Journal of Alloys and Compounds, 2018, 740, 461-469.	2.8	61
68	Influence of Nonstoichiometry on Proton Conductivity in Thin-Film Yttrium-Doped Barium Zirconate. ACS Applied Materials & Interfaces, 2018, 10, 4816-4823.	4.0	18
69	Phase stability and transformation in a light-weight high-entropy alloy. Acta Materialia, 2018, 146, 280-293.	3.8	131
70	Nanoscale Chemical Imaging of Zeolites Using Atom Probe Tomography. Angewandte Chemie - International Edition, 2018, 57, 10422-10435.	7.2	31
71	On spinodal decomposition in alnico - A transmission electron microscopy and atom probe tomography study. Acta Materialia, 2018, 153, 15-22.	3.8	24
72	Effects of temperature on the irradiation responses of Al0.1CoCrFeNi high entropy alloy. Scripta Materialia, 2018, 144, 31-35.	2.6	103

#	Article	IF	CITATIONS
73	Influence of Alloying on α-αʹ Phase Separation in Duplex Stainless Steels. Minerals, Metals and Materials Series, 2018, , 1183-1192.	0.3	0
74	Compositional analysis on the reverted austenite and tempered martensite in a Ti-stabilized supermartensitic stainless steel: Segregation, partitioning and carbide precipitation. Materials and Design, 2018, 140, 95-105.	3.3	51
75	Nanoscale investigation of grain boundary characteristics of single-crystalline-like GaAs films and solar cells on flexible metal substrates. , 2018, , .		Ο
76	Scalable Proximity-Based Methods for Large-Scale Analysis of Atom Probe Data. , 2018, , .		0
77	Quantification of Dopant Profiles in SiGe HBT Devices. , 2018, , .		0
78	Hot Straining and Quenching and Partitioning of a TRIP-Assisted Steel: Microstructural Characterization and Mechanical Properties. Materials Science Forum, 2018, 941, 704-710.	0.3	2
79	Carbon Clustering in Low-Temperature Bainite. Metallurgical and Materials Transactions A: Physical Metallurgy and Materials Science, 2018, 49, 5277-5287.	1.1	21
80	Lattice distortion in a strong and ductile refractory high-entropy alloy. Acta Materialia, 2018, 160, 158-172.	3.8	325
81	Efficient, Parallel At-scale Correlation Analysis for Atom Probe Tomography on Hybrid Architectures. , 2018, , .		2
82	The Influence of Local Distortions on Proton Mobility in Acceptor Doped Perovskites. Chemistry of Materials, 2018, 30, 4919-4925.	3.2	40
83	Evaluation of Carbon Partitioning in New Generation of Quench and Partitioning (Q&P) Steels. Metallurgical and Materials Transactions A: Physical Metallurgy and Materials Science, 2018, 49, 4809-4823.	1.1	14
84	Enhanced strength and ductility of a tungsten-doped CoCrNi medium-entropy alloy. Journal of Materials Research, 2018, 33, 3301-3309.	1.2	51
85	Isolating Clusters of Light Elements in Molecular Sieves with Atom Probe Tomography. Journal of the American Chemical Society, 2018, 140, 9154-9158.	6.6	27
86	Meta-equilibrium transition microstructure for maximum austenite stability and minimum hardness in a Ti-stabilized supermartensitic stainless steel. Materials and Design, 2018, 156, 609-621.	3.3	19
87	Nanoskalige chemische Bildgebung von Zeolithen durch Atomsondentomographie. Angewandte Chemie, 2018, 130, 10580-10593.	1.6	1
88	Unraveling the Effects of Strontium Incorporation on Barite Growth—In Situ and Ex Situ Observations Using Multiscale Chemical Imaging. Crystal Growth and Design, 2018, 18, 5521-5533.	1.4	23
89	Revealing long- and short-range structural modifications within phosphorus-treated HZSM-5 zeolites by atom probe tomography, nuclear magnetic resonance and powder X-ray diffraction. Physical Chemistry Chemical Physics, 2018, 20, 27766-27777.	1.3	18
90	Revealing the beneficial role of K in grain interiors, grain boundaries, and at the buffer interface for highly efficient CuInSe ₂ solar cells. Progress in Photovoltaics: Research and Applications, 2018, 26, 825-834.	4.4	19

#	Article	IF	CITATIONS
91	The effect of carbon on the microstructures, mechanical properties, and deformation mechanisms of thermo-mechanically treated Fe40.4Ni11.3Mn34.8Al7.5Cr6 high entropy alloys. Acta Materialia, 2017, 126, 346-360.	3.8	200
92	Microstructural evolution of single Ni2TiAl or hierarchical NiAl/Ni2TiAl precipitates in Fe-Ni-Al-Cr-Ti ferritic alloys during thermal treatment for elevated-temperature applications. Acta Materialia, 2017, 127, 1-16.	3.8	62
93	Characterization of the effects of different tempers and aging temperatures on the precipitation behavior of Al-Mg (5.25 at.%)-Mn alloys. Materials and Design, 2017, 118, 22-35.	3.3	30
94	Characterizing and modeling the precipitation of Mg-rich phases in Al 5xxx alloys aged at low temperatures. Journal of Materials Science and Technology, 2017, 33, 991-1003.	5.6	27
95	Microstructural and magnetic property evolution with different heat-treatment conditions in an alnico alloy. Acta Materialia, 2017, 133, 73-80.	3.8	51
96	Quantitative assessment of carbon allocation anomalies in low temperature bainite. Acta Materialia, 2017, 133, 333-345.	3.8	56
97	Primary and secondary precipitates in a hierarchical-precipitate-strengthened ferritic alloy. Journal of Alloys and Compounds, 2017, 706, 584-588.	2.8	15
98	Secondary phases in AlxCoCrFeNi high-entropy alloys: An in-situ TEM heating study and thermodynamic appraisal. Acta Materialia, 2017, 131, 206-220.	3.8	292
99	Carbon concentration measurements by atom probe tomography in the ferritic phase of high-silicon steels. Acta Materialia, 2017, 125, 359-368.	3.8	37
100	Accurate Quantification of Si/SiGe Interface Profiles via Atom Probe Tomography. Advanced Materials Interfaces, 2017, 4, 1700622.	1.9	30
101	Rapid Diffusion and Nanosegregation of Hydrogen in Magnesium Alloys from Exposure to Water. ACS Applied Materials & Interfaces, 2017, 9, 38125-38134.	4.0	14
102	Atom-probe study of Cu and NiAl nanoscale precipitation and interfacial segregation in a nanoparticle-strengthened steel. Materials Research Letters, 2017, 5, 562-568.	4.1	29
103	Nanoscale Chemical Imaging of Coking Mechanisms in a Zeolite ZSM-5 Crystal by Atom Probe Tomography. Microscopy and Microanalysis, 2017, 23, 674-675.	0.2	5
104	Heterogeneous Creep Deformations and Correlation to Microstructures in Fe-30Cr-3Al Alloys Strengthened by an Fe2Nb Laves Phase. Metallurgical and Materials Transactions A: Physical Metallurgy and Materials Science, 2017, 48, 4598-4614.	1.1	19
105	Nanoscale tomography reveals the deactivation of automotive copper-exchanged zeolite catalysts. Nature Communications, 2017, 8, 1666.	5.8	105
106	Atom Probe Tomography Unveils Formation Mechanisms of Wear-Protective Tribofilms by ZDDP, Ionic Liquid, and Their Combination. ACS Applied Materials & Interfaces, 2017, 9, 23152-23163.	4.0	34
107	Understanding individual defects in CdTe thin-film solar cells via STEM: From atomic structure to electrical activity. Materials Science in Semiconductor Processing, 2017, 65, 64-76.	1.9	36
108	Recent Progress of Correlative Transmission Electron Microscopy and Atom Probe Tomography for Materials Characterization. Microscopy and Microanalysis, 2017, 23, 692-693.	0.2	0

#	Article	IF	CITATIONS
109	Spinodal Decomposition in an Alnico Alloy. Microscopy and Microanalysis, 2016, 22, 670-671.	0.2	2
110	Quantification of Atomic Arrangements at Heterostructure Interfaces. Microscopy and Microanalysis, 2016, 22, 1502-1503.	0.2	0
111	Considerations and Challenges with Characterizing Si/SiGe Interfaces. Microscopy and Microanalysis, 2016, 22, 1450-1451.	0.2	0
112	Coke Formation in a Zeolite Crystal During the Methanolâ€ŧoâ€Hydrocarbons Reaction as Studied with Atom Probe Tomography. Angewandte Chemie, 2016, 128, 11339-11343.	1.6	16
113	Correlative Energy-Dispersive X-Ray Spectroscopic Tomography and Atom Probe Tomography of the Phase Separation in an Alnico 8 Alloy. Microscopy and Microanalysis, 2016, 22, 1251-1260.	0.2	29
114	Atom Probe Tomography of Interfacial Segregation in CdTe-based Solar Cells. Microscopy and Microanalysis, 2016, 22, 646-647.	0.2	0
115	Effects of Fe concentration on the ion-irradiation induced defect evolution and hardening in Ni-Fe solid solution alloys. Acta Materialia, 2016, 121, 365-373.	3.8	64
116	Structural and compositional dependence of the CdTexSe1â^'x alloy layer photoactivity in CdTe-based solar cells. Nature Communications, 2016, 7, 12537.	5.8	108
117	APT mass spectrometry and SEM data for CdTe solar cells. Data in Brief, 2016, 7, 779-785.	0.5	1
118	Effects of welding and post-weld heat treatments on nanoscale precipitation and mechanical properties of an ultra-high strength steel hardened by NiAl and Cu nanoparticles. Acta Materialia, 2016, 120, 216-227.	3.8	36
119	An atom probe perspective on phase separation and precipitation in duplex stainless steels. Nanotechnology, 2016, 27, 254004.	1.3	43
120	Coke Formation in a Zeolite Crystal During the Methanolâ€ŧoâ€Hydrocarbons Reaction as Studied with Atom Probe Tomography. Angewandte Chemie - International Edition, 2016, 55, 11173-11177.	7.2	74
121	The effect of interstitial carbon on the mechanical properties and dislocation substructure evolution in Fe40.4Ni11.3Mn34.8Al7.5Cr6 high entropy alloys. Acta Materialia, 2016, 120, 228-239.	3.8	373
122	Atomic migration of carbon in hard turned layers of carburized bearing steel. CIRP Annals - Manufacturing Technology, 2016, 65, 85-88.	1.7	8
123	Understanding phase stability of Al-Co-Cr-Fe-Ni high entropy alloys. Materials and Design, 2016, 109, 425-433.	3.3	197
124	Cadmium telluride solar cells: Record-breaking voltages. Nature Energy, 2016, 1, .	19.8	10
125	Characterizing Alnico Alloy by Correlative STEM-EDS Tomography and Atom Probe Tomography. Microscopy and Microanalysis, 2016, 22, 668-669.	0.2	0
126	Visualization of Current and Mapping of Elements in Quantum Dot Solar Cells. Advanced Functional Materials, 2016, 26, 895-902.	7.8	3

#	Article	IF	CITATIONS
127	Nanoscale doping profiles within CdTe grain boundaries and at the CdS/CdTe interface revealed by atom probe tomography and STEM EBIC. Solar Energy Materials and Solar Cells, 2016, 150, 95-101.	3.0	35
128	The role of silicon, vacancies, and strain in carbon distribution in low temperature bainite. Journal of Alloys and Compounds, 2016, 673, 289-294.	2.8	10
129	Structure and dynamics of shear bands in amorphous–crystalline nanolaminates. Scripta Materialia, 2016, 110, 28-32.	2.6	23
130	CdSe1_xTex Phase Segregation in CdSe/CdTe Based Solar Cells. Microscopy and Microanalysis, 2015, 21, 691-692.	0.2	2
131	Ferritic Alloys with Extreme Creep Resistance via Coherent Hierarchical Precipitates. Scientific Reports, 2015, 5, 16327.	1.6	80
132	Controllable Growth of Perovskite Films by Roomâ€Temperature Air Exposure for Efficient Planar Heterojunction Photovoltaic Cells. Angewandte Chemie - International Edition, 2015, 54, 14862-14865.	7.2	41
133	Physics of grain boundaries in polycrystalline photovoltaic semiconductors. Journal of Applied Physics, 2015, 117, .	1.1	52
134	Perovskite Solar Cells with Near 100% Internal Quantum Efficiency Based on Large Single Crystalline Grains and Vertical Bulk Heterojunctions. Journal of the American Chemical Society, 2015, 137, 9210-9213.	6.6	246
135	Phase Separation in Lean-Grade Duplex Stainless Steel 2101. Jom, 2015, 67, 2216-2222.	0.9	12
136	Current Enhancement of CdTe-Based Solar Cells. IEEE Journal of Photovoltaics, 2015, 5, 1492-1496.	1.5	49
137	Defect Physics in Photovoltaic Materials Revealed by Combined High-Resolution Microscopy and Density-Functional Theory Calculation. Microscopy and Microanalysis, 2014, 20, 514-515.	0.2	1
138	Understanding Individual Defects in CdTe Solar Cells: From Atomic Structure to Electrical Activity. Microscopy and Microanalysis, 2014, 20, 518-519.	0.2	1
139	S–Te Interdiffusion within Grains and Grain Boundaries in CdTe Solar Cells. IEEE Journal of Photovoltaics, 2014, 4, 1636-1643.	1.5	28
140	Grain-Boundary-Enhanced Carrier Collection in CdTe Solar Cells. Physical Review Letters, 2014, 112, 156103.	2.9	258
141	Disordered grain growth in polycrystalline GaN obtained by the polymer-derived-ceramic route. RSC Advances, 2014, 4, 2634-2639.	1.7	5
142	Direct Electronic Property Imaging of a Nanocrystal-Based Photovoltaic Device by Electron Beam-Induced Current via Scanning Electron Microscopy. Journal of Physical Chemistry Letters, 2014, 5, 856-860.	2.1	12
143	Direct Imaging of Cl―and Cuâ€Induced Short ircuit Efficiency Changes in CdTe Solar Cells. Advanced Energy Materials, 2014, 4, 1400454.	10.2	79
144	Thin Films: Direct Imaging of Cl―and Cuâ€Induced Shortâ€Circuit Efficiency Changes in CdTe Solar Cells (Adv. Energy Mater. 15/2014). Advanced Energy Materials, 2014, 4, .	10.2	0

#	Article	IF	CITATIONS
145	The role of donor-acceptor pairs in the excitation of Eu-ions in GaN:Eu epitaxial layers. Journal of Applied Physics, 2014, 115, .	1.1	45
146	From atomic structure to photovoltaic properties in CdTe solar cells. Ultramicroscopy, 2013, 134, 113-125.	0.8	80
147	Defect roles in the excitation of Eu ions in Eu:GaN. Optics Express, 2013, 21, 30633.	1.7	9
148	Effect of thermal annealing on luminescence properties of Eu,Mg-codoped GaN grown by organometallic vapor phase epitaxy. Applied Physics Letters, 2013, 102, 141904.	1.5	16
149	High-Resolution Confocal Microscopy with Simultaneous Electron and Laser Beam Irradiation. Microscopy and Microanalysis, 2012, 18, 1263-1269.	0.2	8
150	Approaches for high internal quantum efficiency green InGaN light-emitting diodes with large overlap quantum wells. Optics Express, 2011, 19, A991.	1.7	535
151	Near-infrared photoluminescence properties of neodymium in in situ doped AlN grown using plasma-assisted molecular beam epitaxy. Optical Materials Express, 2011, 1, 78.	1.6	10
152	Cathodoluminescence characteristics of linearly shaped staggered InGaN quantum wells light-emitting diodes. , 2011, , .		0
153	Nature and Excitation Mechanism of the Emission-dominating Minority Eu-center in GaN Grown by Organometallic Vapor-phase Epitaxy. Materials Research Society Symposia Proceedings, 2011, 1342, 67.	0.1	4
154	Cathodoluminescence characteristics of linearly-shaped staggered InGaN quantum wells light-emitting diodes. , 2010, , .		0
155	Growths of staggered InGaN quantum wells light-emitting diodes emitting at 520–525 nm employing graded growth-temperature profile. Applied Physics Letters, 2009, 95, .	1.5	150
156	Design and characteristics of staggered InGaN quantum-well light-emitting diodes in the green spectral regime. IET Optoelectronics, 2009, 3, 283-295.	1.8	91
157	Characteristics of staggered InGaN quantum wells light-emitting diodes emitting at 480–525 nm. , 2009, , .		0
158	Complex Nano-Scale Structures for Unprecedented Properties in Steels. Materials Science Forum, 0, 879, 2401-2406.	0.3	2